Estimation of the long-term variability of extreme significant wave height using a time-dependent Peak Over Threshold (POT) model

Fernando J. Méndez,[1] Melisa Menéndez,[1] Alberto Luceño,[2] and Inigo J. Losada[1]

Received 6 October 2005; revised 12 April 2006; accepted 28 April 2006; published 27 July 2006.

[1] Recent evidence suggests long-term changes in the intensity and frequency of extreme wave climate around the globe. These changes may be attributable to global warming as well as to the natural climate variability. A statistical model to estimate long-term trends in the frequency and intensity of severe storm waves is presented in this paper. The model is based on a time-dependent version of the Peak Over Threshold model and is applied to the Washington NOAA buoy (46005) significant wave height data set. The model allows consideration of the annual cycle, trends, and relationship to atmosphere-ocean-related indices. For the particular data set analyzed the inclusion of seasonal variability substantially improves the correlation between the model and the data. Also, significant correlations with the Pacific–North America pattern, as well as long-term trend, are detected. Results show that the model is appropriate for a rigorous analysis of long-term trends and variability of extreme waves and for providing time-dependent quantiles and confidence intervals.

Citation: Méndez, F. J., M. Menéndez, A. Luceño, and I. J. Losada (2006), Estimation of the long-term variability of extreme significant wave height using a time-dependent Peak Over Threshold (POT) model, *J. Geophys. Res.*, *111*, C07024, doi:10.1029/2005JC003344.

1. Introduction

[2] The topic of ocean and coastal climate change poses many statistical challenges, such as the study of changes in the intensity and frequency of severe storms. The analysis of long-term trends and climate variability allows us to assess potential changes of coastal risk flooding as well as to consider variations of extreme value wave climate in the design of maritime works.

[3] There are numerous examples that suggest a non-negligible trend in the intensity and frequency of major storm waves in different seas around the globe. An increase in the intensity and frequency of major storms has been detected in the Northeast Atlantic [see e.g., *Carter and Draper*, 1988; *Grevemeyer et al.*, 2000; *Vikebo et al.*, 2003; *Wang and Swail*, 2001] as well as in the Northeast Pacific Oceans [see, e.g., *Allan and Komar*, 2000; *Graham and Diaz*, 2001; *Wang and Swail*, 2001]. *Gulev and Grigorieva* [2004] detected trends in the last century in the magnitude of observed visual wave heights as well as important correlations between these wave heights and regional climate indices, such as the North Atlantic Oscillation (NAO) [*Hurrell*, 1995] or the Southern Oscillation Index (SOI) [*McPhaden*, 2004]. Recently, *Bromirski et al.* [2005] described the wave spectral energy variability along the northeast Pacific NOAA buoys, obtaining significant correlations with the SOI and the Pacific–North America (PNA) Index [*Wallace and Gutzler*, 1981]; the magnitudes of these correlations depend on the location of each particular buoy.

[4] Several authors have analyzed the nonstationary behavior of extreme wave heights by means of extreme value distributions [e.g., *Carter and Challenor*, 1981; *Morton et al.*, 1997], thus modeling the intra-annual variability. However, the different timescales previously considered by different authors (seasonal and decadal variability, long-term or secular trends) have not been analyzed as a whole using nonstationary extreme value theory. In this paper, we use a time-dependent version of the Peak Over Threshold (POT) model [see, e.g., *Smith*, 2001; *Katz et al.*, 2002; *Davison and Smith*, 1990] to examine trends in the intensity and frequency of extreme wave events.

[5] The paper is organized as follows. First, a brief description of the generalized extreme value and POT models (the so-called generalized Pareto distribution (GPD)–Poisson model) for time-dependent random variables is shown. Second, a description of the data set is given. We use the significant wave height (approximately the average of the highest third of the wave heights in a sea state) to describe the wave climate variation. Third, the parameterization employed in terms of covariates and functions of time is addressed. Next, the model is applied to a particular data set (Washington buoy 46005) showing

[1] Ocean and Coastal Research Group, Universidad de Cantabria, Santander, Spain.
[2] Department of Applied Mathematics, Universidad de Cantabria, Santander, Spain.

0148-0227/06/2005JC003344

the utility of the proposed formulation. Finally, some conclusions are given.

2. Methodology

2.1. GPD-Poisson Model

[6] The simplest model in extreme value theory is the Annual Maxima method (AMM) [see *Coles*, 2001, chap. 3]. In this approach, annual maxima values are assumed to be independent and identically distributed random variables (i.e., random variables whose joint probability distribution is provided by the product of their marginal distributions, which are identical). A useful model for this common distribution is provided by the generalized extreme value (GEV) cumulative distribution function (CDF)

$$H(z;\mu,\psi,\xi) = \exp\left\{-\left[1+\xi\left(\frac{z-\mu}{\psi}\right)\right]^{-1/\xi}\right\}, \quad (1)$$

where $1+\xi(z-\mu)/\psi > 0$, μ is a location parameter, $\psi > 0$ is a scale parameter and ξ is a shape parameter which determines the nature of the tail of the distribution. If $\xi \to 0$, the GEV distribution leads to the Gumbel CDF

$$H(z;\mu,\psi) = \exp\left\{-\exp\left[-\left(\frac{z-\mu}{\psi}\right)\right]\right\}. \quad (2)$$

[7] The main weakness of the AMM comes from using only one data per year, totally disregarding the information in the remaining data. To mitigate this problem, the POT method for independent and identically distributed random variables is used [*Davison and Smith*, 1990]. The basic idea is to choose a high-threshold u and to study the statistical properties of all the exceedances over u; in particular, the number of exceedances over u for a given period of time, the distribution of exceedances within a year, and the amounts by which the threshold is exceeded, i.e., the threshold excesses. We assume that the number of exceedances of the level u in any given year (also valid for other time intervals, see section 2.2) follows a Poisson distribution with annual mean νT, where ν is the event rate (yr^{-1}) and $T = 1$ year, and that the threshold excesses $y > 0$ are modeled using the GPD given by

$$G(y;\sigma,\xi) = \begin{cases} 1-(1+\xi y/\sigma)^{-1/\xi} & \xi \neq 0 \\ 1-\exp(-y/\sigma) & \xi = 0 \end{cases}, \quad (3)$$

where $\sigma > 0$ is a scale parameter and ξ is the shape parameter of the GEV distribution. The combination of the Poisson model for frequency and the GPD model for intensity can be expressed [*Pickands*, 1975; *Smith*, 2001] in a form compatible with the GEV distribution for annual maxima provided that

$$\sigma = \psi + \xi(u-\mu), \quad \nu = (1+\xi(u-\mu)/\psi)^{-1/\xi}. \quad (4)$$

[8] If N exceedances $y_1, y_2, \ldots, y_N$ are observed over a T-year period, the likelihood function for the GPD-Poisson model is expressed as

$$L_{N,y}(\nu,\sigma,\xi) = \frac{(\nu T)^N e^{-\nu T}}{N!}\prod_{i=1}^{N} g(y_i;\sigma,\xi), \quad (5)$$

where g is obtained from G by differentiating with respect to y. After ignoring constants, the corresponding log-likelihood function is

$$l_{N,y}(\nu,\sigma,\xi) = N\log\nu - \nu T - N\log\sigma - \left(1+\frac{1}{\xi}\right)\sum_{i=1}^{N}\log\left(1+\xi\frac{y_i}{\sigma}\right). \quad (6)$$

[9] Maximizing $l_{N,y}(\nu, \sigma, \xi)$ with respect to the vector parameter $\theta = (\nu, \sigma, \xi)$ leads to the maximum likelihood (ML) estimates $(\hat{\nu}, \hat{\sigma}, \hat{\xi})$, and consequently, to the GEV estimates $\hat{\mu}$ and $\hat{\psi}$, by using equation (4).

2.2. Time-Dependent GPD-Poisson Model

[10] An extension of the GPD-Poisson model in section 2.1 is obtained by allowing its parameters to be time-dependent, so that $\nu(t) > 0$, $\sigma(t) > 0$ and $-\infty < \xi(t) < \infty$ may vary throughout the year (e.g., according to parametric expressions to be determined). Accordingly, the GEV distribution inherits time-dependent parameters $-\infty < \mu(t) < \infty$, $\psi(t) > 0$ and $-\infty < \xi(t) < \infty$. The functions $\mu(t)$, $\psi(t)$ and $\xi(t)$ can contain sine waves representing seasonal effects [see, e.g., *Katz et al.*, 2002], linear and/or exponential terms representing long-term trends, and covariates representing environmental processes (e.g., El Niño), among others.

[11] The log-likelihood for this model can be obtained from the daily version of equation (6) (i.e., the equation obtained for a time interval of one day, instead of one year). If the N exceedances $y_1, y_2, \ldots, y_N$ are observed at days $t_1, t_2, \ldots, t_N$ over a T-year period, the log-likelihood function for the time-dependent GPD-Poisson model is expressed as,

$$l_{y,t}(\theta) = \sum_t \left\{\eta_{t_i}\log\nu(t_i) - \frac{\nu(t_i)}{T_S} - \eta_{t_i}\log\sigma(t_i) - \eta_{t_i}\left(1+\frac{1}{\xi(t_i)}\right)\cdot\log\left(1+\xi(t_i)\frac{y_i}{\sigma(t_i)}\right)\right\}, \quad (7)$$

where $\sigma(t)$ and $\nu(t)$ are related to the GEV parameters using the time-dependent version of equation (4); η_{t_i} equals 1 if there is an exceedance on day t_i and 0 otherwise; T_s is a time scaling constant so that $T_s = 365.25$ (for a daily time interval); y_i is the threshold excess on day t_i; θ is a vector of regression parameters; and the sum over t is extended to all the days with data available (i.e., days without data are omitted).

[12] As shown in section 3, the vector θ may contain more than 10 regression parameters for some of the proposed models, making it difficult to maximize the log-likelihood function. Therefore an efficient global optimization procedure has been used, namely the SCE-UA algorithm [*Duan et al.*, 1992], which is widely used in the calibration of

highly nonlinear problems. The SCE-UA optimization scheme has been applied successfully in all the cases analyzed in this study.

2.3. Confidence Intervals

[13] Approximate standard errors for the estimators and confidence intervals for the regression parameters are obtained using standard likelihood theory [see, e.g., *Coles*, 2001]. For a large sample size n and assuming that the proposed model is valid, the distribution of the ML estimators $\hat{\theta}$ is approximately multivariate normal with mean θ (the true parameter values) and covariance matrix given by the inverse of the observed information matrix $I_O(\theta)$,

$$I_O(\theta) = -\frac{\partial^2 l(\theta)}{\partial\theta_i \partial\theta_j}, \qquad i,j = 1, ..., p, \tag{8}$$

evaluated at $\theta = \hat{\theta}$. If an arbitrary term in the inverse of $I_O(\theta)$ is s_{ij}, the square root of the diagonal entry s_{ii} is approximately the standard error, $se(\hat{\theta}_i)$, of the ML estimator $\hat{\theta}_i$. Therefore confidence intervals for θ_i can be obtained in the form $[\hat{\theta}_i - z_\alpha se(\hat{\theta}_i), \hat{\theta}_i + z_\alpha se(\hat{\theta}_i)]$, where $z_{0.95} = 1.96$ gives a 95% confidence interval.

2.4. Model Diagnostics

[14] There are a number of procedures for model checking when data are assumed to be identically distributed, but they are not directly applicable to time-dependent random variables unless some modifications are performed. One possibility is to standardize the data, conditional on the fitted parameter values. *Smith* [2001] provides a detailed discussion of graphical procedures to examine the goodness of fit of extreme value models for frequency (Z statistic) and for intensity (W statistic). For given exceedance days $t_1, \ldots, t_k, \ldots, t_N$ and corresponding threshold excess $y_1, \ldots, y_k, \ldots, y_N$, the Z statistic is the cumulative event rate of the Poisson process between consecutive exceedances defined as

$$Z_k = \int_{t_{k-1}}^{t_k} \hat{\nu}(t)dt, \tag{9}$$

where $\hat{\nu}(t)$ is the event rate of the Poisson process at t, estimated according to the time-dependent version of equation (4). If the model is correct, $Z_1, Z_2, \ldots, Z_N$ should be exponential random variables with mean 1. The W statistic is given by

$$W_k = \frac{1}{\hat{\xi}(t_k)} \log\left[1 + \frac{\hat{\xi}(t_k) y_k}{\hat{\psi}(t_k) + \hat{\xi}(t_k)(u - \hat{\mu}(t_k))}\right], \tag{10}$$

where $\hat{\mu}(t)$, $\hat{\psi}(t)$, $\hat{\xi}(t)$ are the estimated location, scale and shape time-dependent GEV parameters, respectively. Again, if the model is correct, $W_1, W_2, \ldots, W_N$ should also be exponential variables with mean 1. Diagnostic probability-probability (PP) and quantile-quantile (QQ) plots can be made for both Z and W statistics. If the suggested model is adequate, the PP and QQ plots should consist of points close to the unit diagonal. It is important to note that both plots must be checked simultaneously as they contain the same information but on different scales. The application of both diagnostic plots is performed in section 5 for the best obtained model for the Washington buoy (46005) significant wave height data set (see Figure 4).

2.5. Model Selection

[15] There are many potential models with different formulations of the extreme value parameters as functions of time and other covariates. Therefore the selection of the simplest possible model (following the principle of parsimony) that fits the data sufficiently well is important.

[16] Model selection can be performed using the likelihood ratio test. With nested models $M_A \subset M_B$ (M_B with p parameters and M_A with p-k parameters), we can assure that model M_B explains substantially (at the α level of significance) more variability in the data than M_A if

$$[l_B(M_B) - l_A(M_A)] > \frac{1}{2}\chi^2_{k,1-\alpha}, \tag{11}$$

where $l_B(M_B)$ and $l_A(M_A)$ are the maximized log-likelihood functions under models M_B and M_A, respectively, and $\chi^2_{k,1-\alpha}$ is the $1 - \alpha$ quantile of the χ^2 distribution with k degrees of freedom.

[17] If the number of nested candidate models is large, the quality of the models can be assessed systematically by minimizing a penalty function such as the Akaike Information Criteria (AIC) [*Akaike*, 1973],

$$\mathrm{AIC} = -2\hat{l}(p) + 2p, \tag{12}$$

where p is the number of parameters and $\hat{l}(p)$ is the maximum of the log-likelihood resulting from each model. This criterion assesses the quality of each model by making a compromise between obtaining a good fit, which is measured by how small the resulting $-\hat{l}(p)$ is, and using a simple model, where simpler models use fewer parameters than complex models. Therefore the smaller the criterion, the better the model.

2.6. Estimation of Quantiles

[18] Estimates of the time-dependent extreme quantiles are obtained by inverting equations (1)–(2)

$$\hat{y}_q(t) = \begin{cases} \hat{\mu}(t) - \dfrac{\hat{\psi}(t)}{\hat{\xi}(t)}\left\{1 - [-\log(1-q)]^{-\hat{\xi}(t)}\right\}, & \hat{\xi}(t) \neq 0, \\ \hat{\mu}(t) - \hat{\psi}(t)\log[-\log(1-q)], & \hat{\xi}(t) = 0, \end{cases} \tag{13}$$

where $\hat{y}_q(t)$ is the time-dependent return level associated with the return period $1/q$ (years) and $0 < q < 1$. Confidence intervals can be obtained, using the asymptotic normality property of ML estimators, by the delta method. This method expands the function $\hat{y}_q$ in a neighborhood of the ML estimates $\hat{\theta}$, using a one-step Taylor approximation, and

then takes the variance [*Rice*, 1994]. The standard error of $\hat{y}_q$ can then be estimated from

$$se\left(\hat{y}_q(t)\right) = \left(\sum_{i=1}^{p}\sum_{j=1}^{p}\frac{\partial\hat{y}_q(t)}{\partial\theta_i}\frac{\partial\hat{y}_q(t)}{\partial\theta_j}s_{ij}\right)^{1/2}, \qquad (14)$$

where the partial derivatives are evaluated at $\hat{\theta}$.

3. Regression Model

[19] Likelihood-based methods allow modeling different factors to explain the variability of the data and the nonstationarity of the GEV or GPD-Poisson parameters. Amongst these factors, we shall consider the annual variability (seasonality), a likely long-term trend and interannual climate variability effects explained by global meteorological indices.

[20] We express the model in terms of the GEV parameters using the time-dependent version of equation (4) to relate the GPD-Poisson parameters to the equivalent GEV parameters. Therefore a number of possible regression models can be expressed in terms of the time-dependent location, scale, and shape parameter of the GEV distribution. In this paper, we shall assume that the shape parameter is constant (i.e., $\xi(t) = \xi_o$). Seasonality will be modeled through the seasonal location parameter

$$\mu_S(t) = \beta_o + \beta_1\cos(2\pi t) + \beta_2\sin(2\pi t) + \beta_3\cos(4\pi t) + \beta_4\sin(4\pi t), \qquad (15)$$

where β_o is a mean value, t is given in years, β_1 and β_2 are the coefficients corresponding to the annual cycle and β_3 and β_4 are the coefficients corresponding to the semiannual cycle. Similarly, a long-term trend is incorporated in the model by multiplying the seasonal location parameter by $\exp(\beta_{LT}t)$, where β_{LT} is a trend. The exponential terms have the property that, for small long-term variations (say, $\beta_{LT} \rightarrow 0$), the exponential $\exp(\beta_{LT}t)$ is approximately equivalent to $(1 + \beta_{LT}t)$, so that 100 β_{LT} can be considered as a yearly percentage of variability, when t is given in years. For example, if $\beta_{LT} = 0.001$ yr^{-1}, this corresponds to an increase in the location parameter of about 0.1% per year. More complex models can be built allowing, for instance, a quadratic law for the long-term trend, $\exp(\beta_{LT}t + \beta_{LT_2}t^2)$, or different trends for the mean value and the seasonal component, parameterized as $\beta_0\exp(\beta_{LT}t) + [\beta_1\cos(2\pi t) + \ldots]\exp[(\beta_{LT} + \beta_{LTS})t]$, where β_{LTS} represents an extra term associated to the seasonal long-term trend. Nevertheless, for the particular data set analyzed, the inclusion of β_{LT_2} and β_{LTS} was far from significant.

[21] We introduce interannual climate variability in the model by means of linear functions of regional climate indices that represent atmospheric patterns related to teleconnections from the tropics to the midlatitudes associated with the El Niño–Southern Oscillation (ENSO), such as the SOI [*McPhaden*, 2004] or PNA [*Wallace and Gutzler*, 1981]. SOI is based on the standard deviation of the normalized pressure difference between Darwin (Australia) and Tahiti (French Polynesia), varying usually between −4 and +4, with negative values during El Niño events and positive values during La Niña events. The PNA pattern involves a negative pressure anomaly over the northern Pacific south of Alaska, combined with a positive anomaly over the western mountain regions of North America and another negative anomaly over the eastern U.S. and adjacent Atlantic waters. This index is a measure of the strength and duration of the westerly winds and the position of the jet stream, all of these factors being of importance in the conditions of wave generation which depends on wind speeds, storm duration and fetch lengths [*Hasselmann et al.*, 1976].

[22] It would also be interesting to account for changes in forcing associated with Pacific Decadal Variability (the Pacific Decadal Oscillation, PDO) [*Mantua et al.*, 1997]. However, the relatively short time series available makes it impossible to obtain a reliable correlation with this index. Obviously, disregarding this decadal-scale variability due to the PDO may introduce some unavoidable uncertainty in the long-term trend estimate $\hat{\beta}_{LT}$.

[23] Consequently, in this study we shall entertain the SOI and PNA indices as possible covariates to explain data variability. In this respect, our approach is similar to that of *Allan and Komar* [2000], who used a stepwise multiple regression analysis between the residual winter wave heights and SOI and PNA-related indices. Thus the SOI and PNA effects may be introduced in equation (15) as new terms β_{SOI} SOI(t) and β_{PNA} PNA(t), respectively. Consequently, a possible expression for the location parameter is

$$\mu(t) = \mu_S(t)\exp(\beta_{LT}t) + \beta_{SOI}\mathrm{SOI}(t) + \beta_{PNA}\mathrm{PNA}(t). \qquad (16)$$

A similar analysis can be performed for the scale parameter, giving

$$\psi(t) = \psi_S(t)\exp(\alpha_{LT}t) + \alpha_{SOI}\mathrm{SOI}(t) + \alpha_{PNA}\mathrm{PNA}(t), \qquad (17)$$

where $\psi_S(t) = \alpha_o + \alpha_1\cos(2\pi t) + \alpha_2\sin(2\pi t)$, α_o is a mean value, α_i, $i = 1, 2$ are the seasonal coefficients, α_{LT} is a long-term trend and α_{SOI} and α_{PNA} allow for the SOI and PNA effects in the scale parameter, respectively. It must be noted that the parameterization of the time-dependent GEV parameters can be adapted depending on the geophysical variable and the location of each particular case.

4. Data

4.1. Buoy Data

[24] Data from Washington buoy (46005) provided by NOAA are used in the analysis. The buoy is located about 400 Km away from the west coast of the United States (46.05°N, 131.02°W) at 2780 meters depth. Mean wave climate is characterized at this particular site by annual mean significant wave height (H_s) of 2.7 m and annual mean period of 7s. This data set is known to have a significant trend for annually averaged values of H_s (0.021 m yr^{-1} since 1978) [*Gower*, 2002] as well as for the maximum annual H_s (0.108 m yr^{-1} since 1978. These values, obtained following a least squares linear regression technique, are reported by *Komar and Allan* [2004]). A 29-year-long (1976–2004) H_s data set is available, although with some gaps. The gaps are usually in the winter season (ONDJFM), invalidating the use of the whole year for the

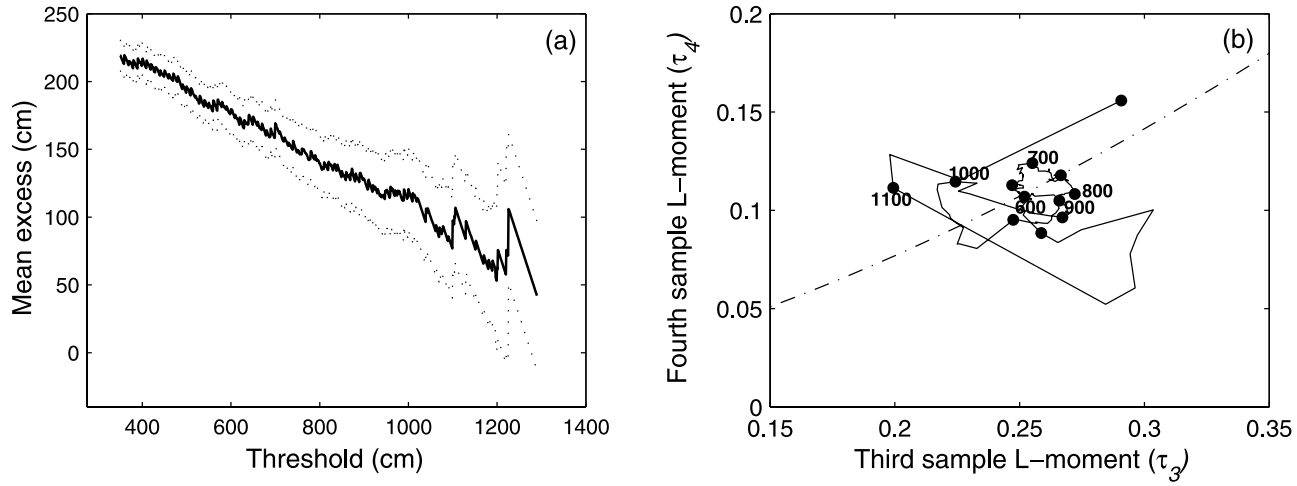

Figure 1. (a) Mean excess plot with 95% confident intervals (dotted lines) and (b) *L*-moment plot for exceedances of H_s over selected thresholds (from 600 to 1100 cm) with the theoretical GPD curve (dash-dotted line) at Washington buoy (46005).

AMM. Thus, for the AMM we remove from the analysis a complete year if any of the months of the winter season of that particular year has less than 40% of data. However, the time-dependent GPD-Poisson model allows the consideration of most of the available data (a filter is used to remove days with less than 3 samples d^{-1}). After applying this filter to the initial 9372 days, 8661 days are available.

4.2. Selection of the Threshold Value and the Time Span

[25] Two important issues that must be overcome when using the peak over threshold approach are the selection of the threshold u and the minimum time span Δt that will be required to assume the independence of consecutive storm events. Both the truncation value and the time span affect the results in terms of the frequency and the exceedance estimates [see, e.g., *Coles*, 2001; *Beguería*, 2005; *Luceño et al.*, 2006].

[26] The selection of the threshold u implies a balance between bias and variance. Too low a threshold will likely violate the basis of the model, causing bias; too high a threshold will identify few extremes, leading to high variance. The usual recommendation is to adopt as low a threshold as possible so that the GPD model provides a reasonable approximation to the exceedances.

[27] Concerning time span, Δt is chosen as the optimal compromise between the minimum time interval over which the Poisson process may be assumed to be valid [see *Luceño et al.*, 2006], the "physical" time interval to guarantee the independency between consecutive storms, and the length of the time series. A wide range of values of Δt has been found in the literature (e.g., *Morton et al.* [1997] used Δt =1.25 days, whereas *Guedes Soares and Scotto* [2004] chose Δt = 20 days). A number of authors have analyzed the patterns of atmospheric low-frequency variability trying to obtain the length of the storms [see, e.g., *Corti et al.*, 1997; *Chen and Yoon*, 2002] for different areas around the globe. For the northeast Pacific, this length is usually associated to persistence large-scale atmospheric phenomena (blocking episodes) with about 30 blocked days per winter and an average duration of 11 days [*Corti et al.*, 1997]. Moreover, this blocking activity is affected by interannual climate variability. This means that Δt should be time-dependent, making difficult the selection of the independent storm events. However, this analysis is outside the scope of this work. We have tested values between 3 and 10 days and, although the Poisson assumption is slightly better satisfied with Δt = 6 days, we choose Δt = 3 days because, as will be shown in section 5, the conclusions were almost the same and the shorter time span gives a higher number of extreme events and slightly smaller confidence intervals.

[28] Different a priori exploratory methods based on sample data (mean excess plot, *L* moment plot) as well as a posteriori methods (stability of the parameter estimates across a range of different thresholds, PP and QQ plots for *Z* and *W* statistics) can be used to choose the threshold and the time span. The mean excess plot, defined as the mean of all excesses over the threshold (see details given by *Davison and Smith* [1990] or *Smith* [2001]) for independent extreme events (using a time span of 3 days) and the 95% confidence intervals based on the approximate normality of sample means are shown in Figure 1a. A clear linear trend appears in the series from the lowest values of the threshold up to the highest values (about 920 cm) where the plot becomes unstable.

[29] The *L* moment plot (Figure 1b) shows the sample ($\hat{\tau}_3$, $\hat{\tau}_4$) *L* moment estimates (see also details given by *Beguería* [2005]) for a given set of increasing threshold values. The *L* moments are linear functions of the probability-weighted moments of the sample [*Hosking and Wallis*, 1987]. The curve described by the theoretical GPD *L* moments, derived by *Hosking* [1990], is also plotted. The deviations from this theoretical curve help to select the threshold. The points (every point represents a given threshold u) describe an elliptical trajectory about the GPD curve, which behaves as an attractor of the process until high values of the threshold are reached (at which the variability of the trajectories increase considerably because of the fast

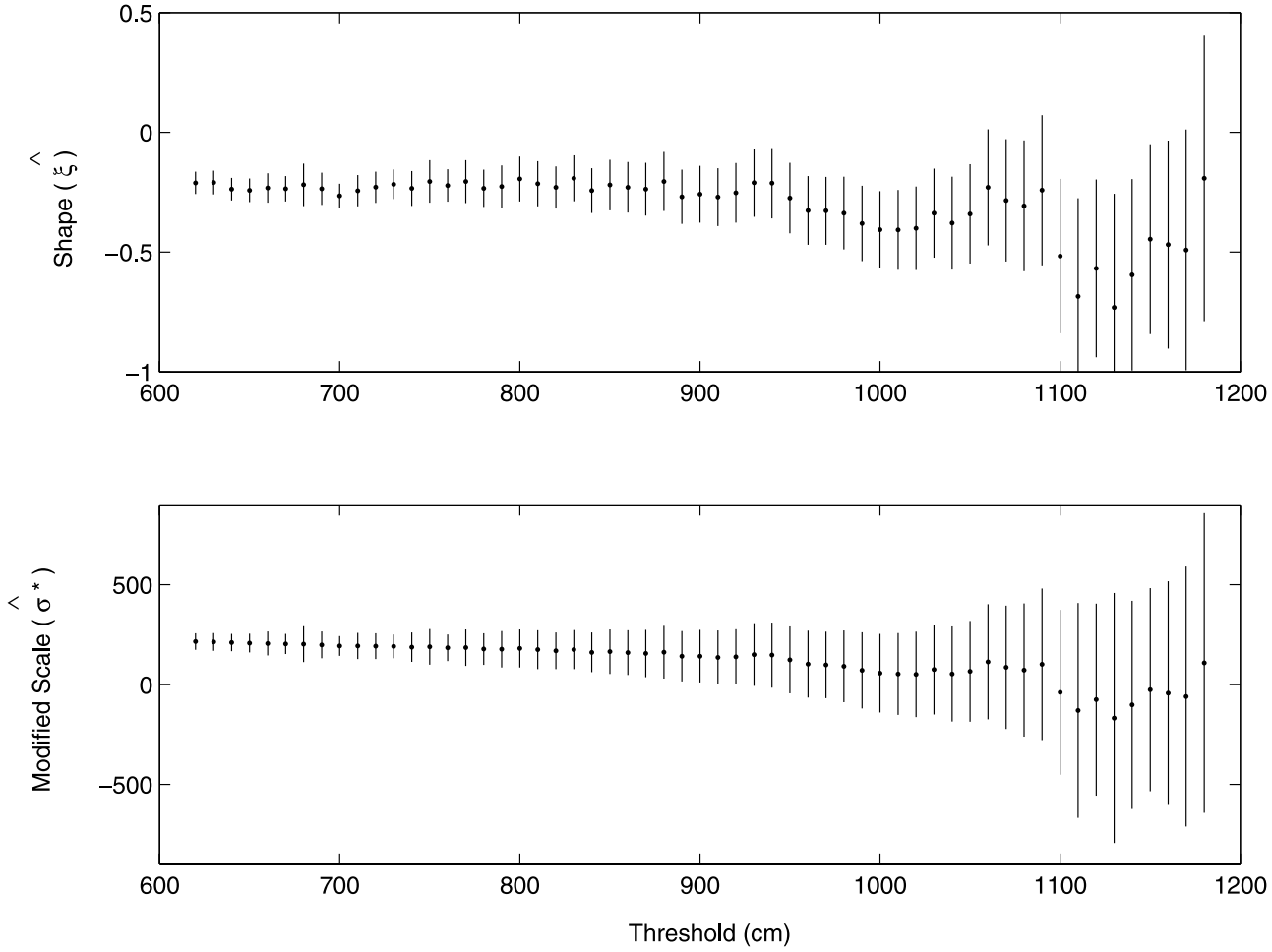

Figure 2. Model shape and modified scale GPD parameters (points) and 95% confidence intervals (vertical bars) versus threshold for 46005 H_s data. Time span is Δt = 3 days.

decreasing number of exceedances). The range $600 < u < 900$ cm appears to be compatible with the GPD model.

[30] Additionally, and using the simpler GPD model of section 2.1, an analysis of the stability of the parameters is carried out. For every value of the threshold u, we calculate the parameter estimates $\hat{\sigma}_u$ and $\hat{\xi}_u$, and reparameterize the GPD scale parameter as $\hat{\sigma}^* = \hat{\sigma}_u - \hat{\xi}_u u$. Standard errors for $\hat{\sigma}^*$ are obtained using the delta method (see details given by *Coles* [2001]). The plots of $\hat{\sigma}^*$ and $\hat{\xi}_u$ and the associated standard errors against u are shown in Figure 2. As in the mean excess plot and the L moment plot, perturbations are also apparent here for $u > 900$ cm.

[31] After inspection of these plots, we conclude that a threshold of about 800 is adequate for the GPD model. Finally, we choose u = 810 cm (which corresponds to the 99.5% percentile of the empirical H_s distribution).

[32] Annual maximum H_s and exceedances over threshold u = 810 cm are shown in Figure 3. Annual maxima values are marked by a circle. The minimum time span to assure independence between consecutive storms is chosen to be 3 days. For this case, the annual maximum series is composed of T = 23 years and the number of independent exceedances is N = 125 (5.4 storms per year). Simple inspection of the time series reveals an important positive trend, not only in the intensity but also in the frequency of major storms.

5. Results

[33] In order to assess the importance of the different processes which explain the long-term trends, various submodels obtained from equations (16) and (17) were analyzed for different combinations of the model parameters. Table 1 shows the set of parameters used by each submodel together with the ML estimates of these parameters, the number of parameters p, the maximum attained by the log-likelihood function for every submodel and the AIC value. It should be noted that the maxima of the log-likelihood functions obtained from models GEV_0 and GEV_1 are not to be compared with the corresponding values for models GPD-P_0 to GPD-P_6 because the former are based on a much smaller sample size.

5.1. Models Without Climate Indices

[34] Comparing GEV_1 model versus GEV_0, it is remarkable that the inclusion of the long-term trend ($\hat{\beta}_{LT} = 0.0106$ yr^{-1}) is significant at the 0.05 level of significance since the difference between the maxima of the log-likelihood func-

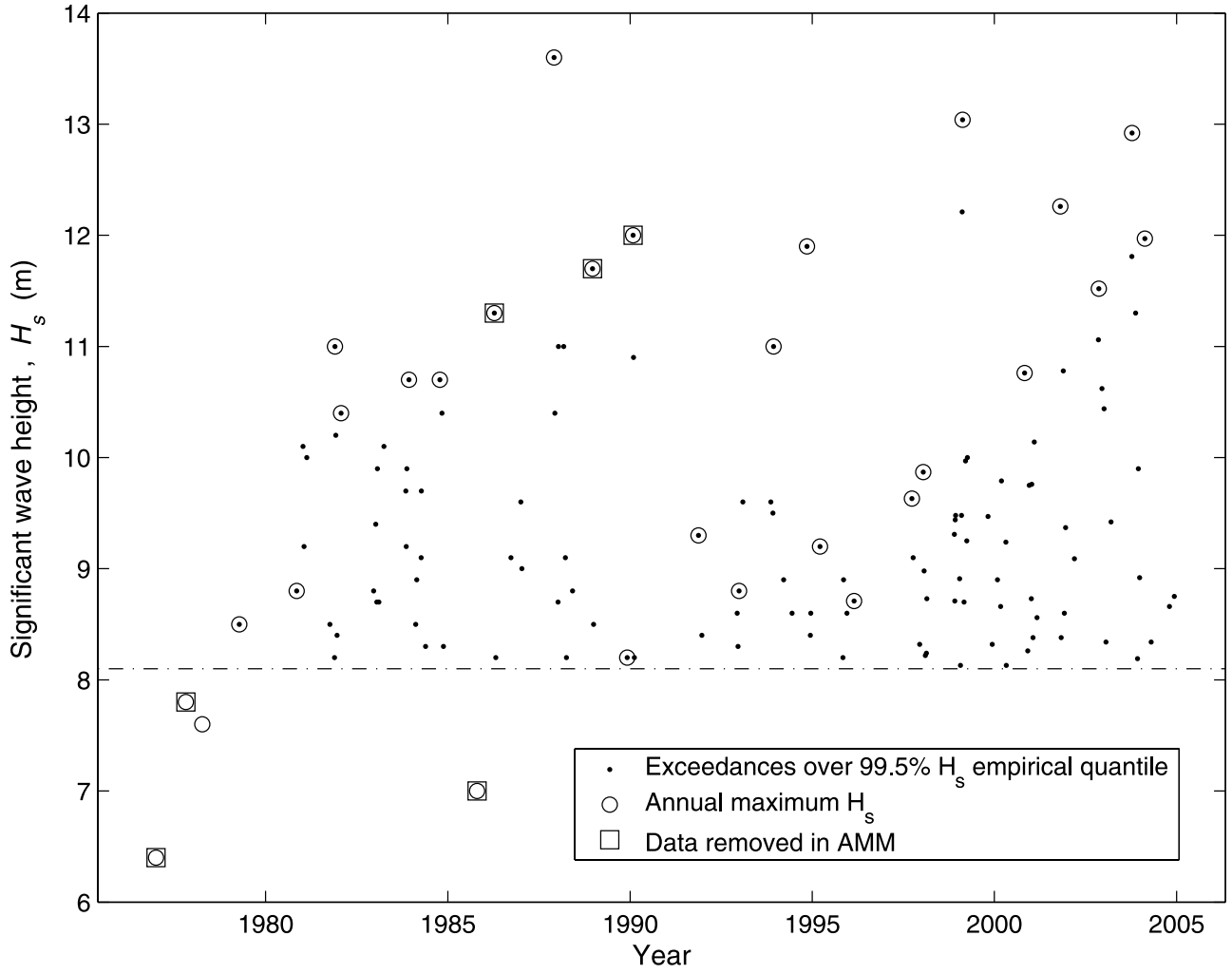

Figure 3. Annual maxima series and peaks of exceedances over the 99.5% H_s empirical quantile. Washington buoy (46005).

Table 1. Summary of the Results for Different Models: ML Estimates for the Time-Dependent GEV Parameters[a]

ML Estimate	GEV0	GEV-1	GPD-P0	GPD-P1	GPD-P2	GPD-P3	GPD-P4	GPD-P5	GPD-P6
$\hat{\beta}_0$	985.5673	846.5659	1049.317	983.746	879.900	954.280	878.762	876.220	886.476
$\hat{\beta}_1$	...	...	...	...	269.191	...	254.969	260.584	277.962
$\hat{\beta}_2$	...	...	...	...	47.134	...	41.153	22.608	49.926
$\hat{\beta}_3$	...	...	...	...	−47.847	...	−49.337	−48.793	−48.353
$\hat{\beta}_4$	...	...	...	...	−75.199	...	−76.353	−90.889	−78.506
$\hat{\beta}_{LT}$	...	0.0106	...	0.00453	0.00404	0.00500	0.00361	0.00354	0.00156
$\hat{\beta}_{LT_2}$	...	...	...	...	...	...	...	...	0.068
$\hat{\beta}_{SOI}$	...	...	...	...	...	30.624	23.941	27.564	...
$\hat{\beta}_{PNA}$	...	...	...	...	...	152.567	86.221	90.394	...
$\hat{\alpha}_0$	157.6126	124.6533	119.807	118.643	106.233	123.079	108.054	111.274	106.229
$\hat{\alpha}_1$	...	...	...	...	...	...	...	−2.609	...
$\hat{\alpha}_2$	...	...	...	...	...	...	...	−17.396	...
$\hat{\xi}_0$	−0.2593	−0.0876	−0.215	−0.219	−0.217	−0.140	−0.195	−0.185	−0.216
p	3	4	3	4	8	6	10	12	9
l	−149.5461	−146.29	−658.216	−655.192	−593.592	−641.268	−589.127	−587.906	−593.520
AIC			1322.433	1318.384	1203.183	1294.536	1198.255	1199.811	1205.040

[a]Location parameters include the following: β_0 is a mean value, β_1 and β_2 are the coefficients corresponding to the annual cycle, β_3 and β_4 are the coefficients corresponding to the semiannual cycle, β_{LT} is a long-term trend, β_{LT_2} models a quadratic law for the long-term trend, and β_{SOI} and β_{PNA} are linear coefficients for the SOI and PNA climate indices, respectively. Scale parameters include the following: α_0 is a mean value, α_1 and α_2 are the coefficients corresponding to the annual cycle. Shape parameters include the following: ξ_0, number of parameters (p), maximum log likelihood function (l), and AIC criteria (equation (12)).

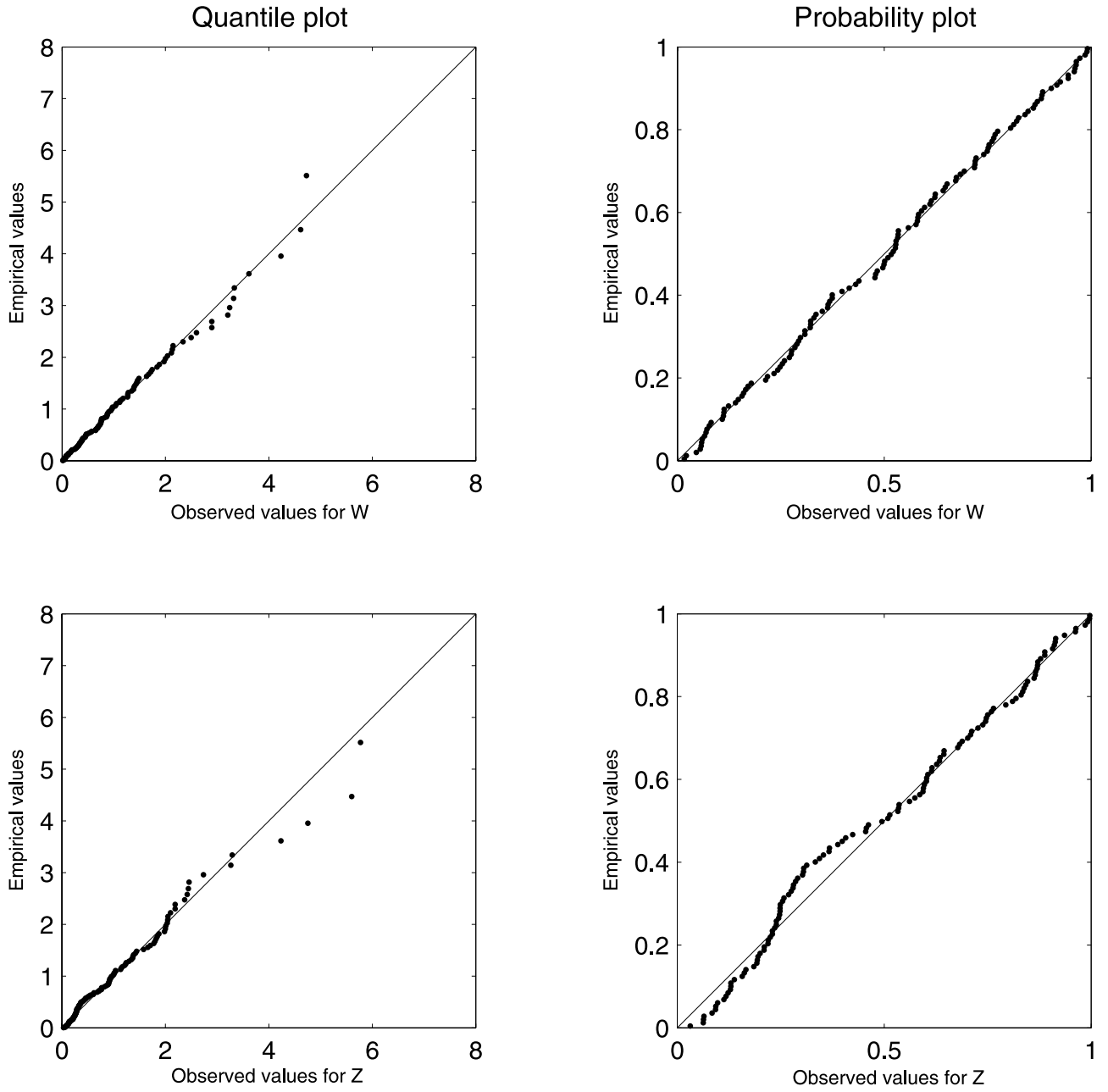

Figure 4. Diagnostic QQ and PP plots for Z- and W-statistics (see equations (9) and (10)) corresponding to model GPD-P_4. Points close to the diagonal suggest an adequate goodness of fit.

tions is greater than 0.5 $\chi^2_{1,095} = 1.92$. This implies an annual trend of approximately $\hat{\beta}_0\hat{\beta}_{LT} = 8.5$ cm yr^{-1}. If we compare GPD-P_1 model versus GPD-P_0 we also find that the trend is significant, but the annual trend is now about $\hat{\beta}_0\hat{\beta}_{LT} = 4.4$ cm yr^{-1}.

[35] The improvement of the fit is impressive as judged by the value of l when seasonality is considered. Thus, comparing model GPD-P_2 (that includes annual and semi-annual cycles for the location parameter) versus GPD-P_1, we obtain an increase of more than 61 units in the maximum log-likelihood function, which is significant at the 0.000001 level. The annual trend is even smaller ($\hat{\beta}_0\hat{\beta}_{LT} = 3.5$ cm yr^{-1}). We have also tried a parabolic trend ($\beta_{LT}t + \beta_{LT_2}t^2$) in model GPD-$P_6$, but it is not statistically significant at the 0.05 level.

5.2. Models With Climate Indices

[36] This model can be adapted to account not only for long-term trends but also for decadal climate variability. Thus model GPD-P_3 considers a long-term trend and both the SOI and the PNA indices, which are known to be highly correlated with the wave climate at buoy 46005 [see, e.g., *Allan and Komar*, 2000]. Comparing model GPD-P_3 versus model GPD-P_1, it is seen that the inclusion of SOI and PNA in the location parameter improves l about 14 units, which is significant at the 0.00001 level.

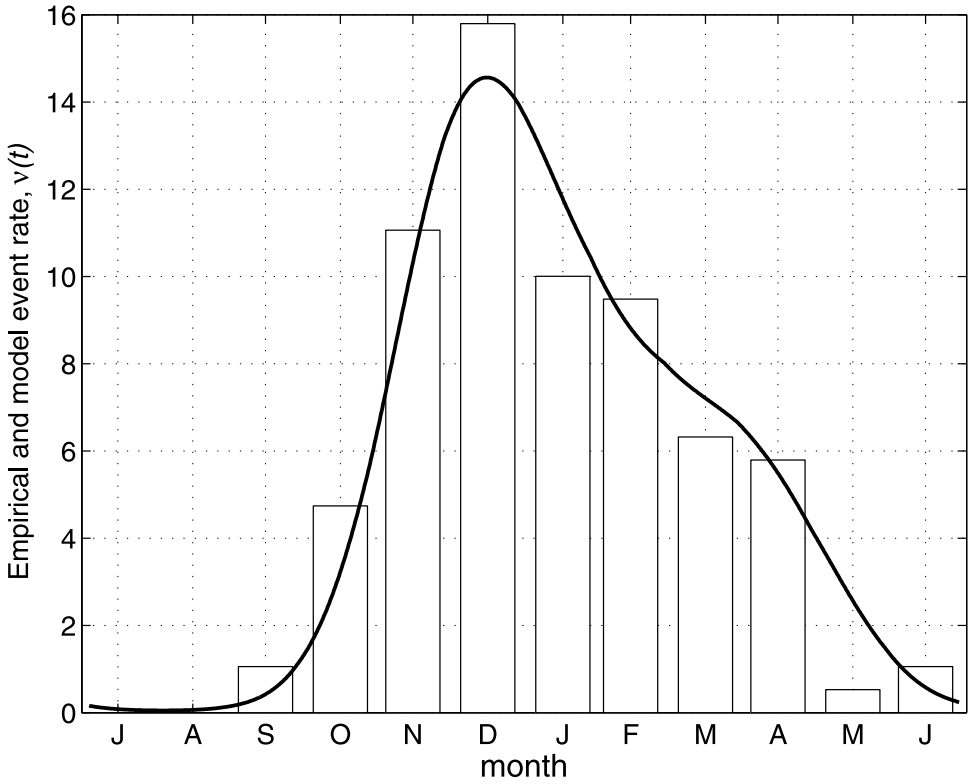

Figure 5. Histogram of the time of occurrence of threshold excesses (bars) and time-dependent event rate $\hat{\nu}(t)$ within a year in an average year (solid line), according to model GPD-P_4.

[37] The inclusion of seasonality in the location parameter (annual and semiannual cycles) in model GPD-P_4 helps to explain more data variability as can be seen in the maximum log-likelihood functions (more than 52 units).

[38] We also tested the inclusion of nonstationarity in the scale parameter by including an annual cycle (equation (17)), $\psi_S(t) = \alpha_0 + \alpha_1 \cos(2\pi t) + \alpha_2 \sin(2\pi t)$ (model GPD-P_5), but (α_1, α_2) were not significant at the 0.05 level. Other possible models including α_{LT}, α_{SOI} and α_{PNA} were not significant.

5.3. Selected Model

[39] Therefore, for the particular data set analyzed, model GPD-P_4 can be considered the best choice (note also that its AIC is the lowest, supporting the selection of GPD-P_4 model). For this particular model, the number of parameters is $n = 10$ and the vector parameter is $\theta = (\beta_0, \beta_1, \beta_2, \beta_3, \beta_4, \beta_{LT}, \beta_{PNA}, \beta_{SOI}, \alpha_0, \xi_0)$. Thus we obtain constant values for the scale and shape parameters ($\psi(t) = \alpha_0$, $\xi(t) = \xi_0$) and the time-dependent location parameter is expressed as,

$$\mu(t) = [\beta_o + \beta_1 \cos(2\pi t) + \beta_2 \sin(2\pi t) + \beta_3 \cos(4\pi t) + \beta_4 \sin(4\pi t)] \cdot \exp(\beta_{LT} t) + \beta_{SOI}\mathrm{SOI}(t) + \beta_{PNA}\mathrm{PNA}(t) \quad (18)$$

[40] For this particular model, every unit of PNA explains 86 cm of the variation of the data. SOI seems to play a minor role, slightly affecting during La Niña events (positive SOI values are associated with El Niño, while negative SOI values indicate La Niña). These correlations with PNA and SOI indices are in coincidence with previous works by *Allan and Komar* [2000] and *Bromirski et al.* [2005] for the residual (or anomaly) winter wave energy.

[41] The estimated long-term trend is not affected much by the decadal variability, giving an annual trend of $\hat{\beta}_0\hat{\beta}_{LT} = 3.2$ cm yr^{-1}. It is interesting to note that, for the particular data set analyzed, the long-term trends of these statistical extreme value models are significantly smaller than previous results using a least squares linear regression technique for annual maximum series for the same data set (10.8 cm yr^{-1}) [*Komar and Allan*, 2004]. The authors believe that the proposed model gives a more reliable estimate of the long-term trend.

5.4. Sensitivity of the Best Model

[42] We have used the Z and W statistics described in section 2.4 to test the goodness of the fit of the model. As an example, Figure 4 shows the results for model GPD-P_4. The fit of the GPD model is remarkably good (PP and QQ plots for W statistic) but the Poisson distribution (PP and QQ plots for Z statistic) does not fit so well. This is attributable to the time span $\Delta t = 3$ days chosen between independent storms. Better fits for the Z statistics are achieved using $\Delta t = 6$ days but, as indicated previously, we prefer to present the results for $\Delta t = 3$ days to avoid the loss of useful extreme data (11% of data), considering that the conclusions are very similar otherwise. The differences are less than 10% for all the parameter estimates. As an example, for $\Delta t = 6$ days the long-term trend for model GPD-P_4 is $\hat{\beta}_0\hat{\beta}_{LT} = 3.0$ cm yr^{-1} (about a 6% difference). The Poisson process assumption is an open question that has recently been addressed by *Luceño et al.* [2006].

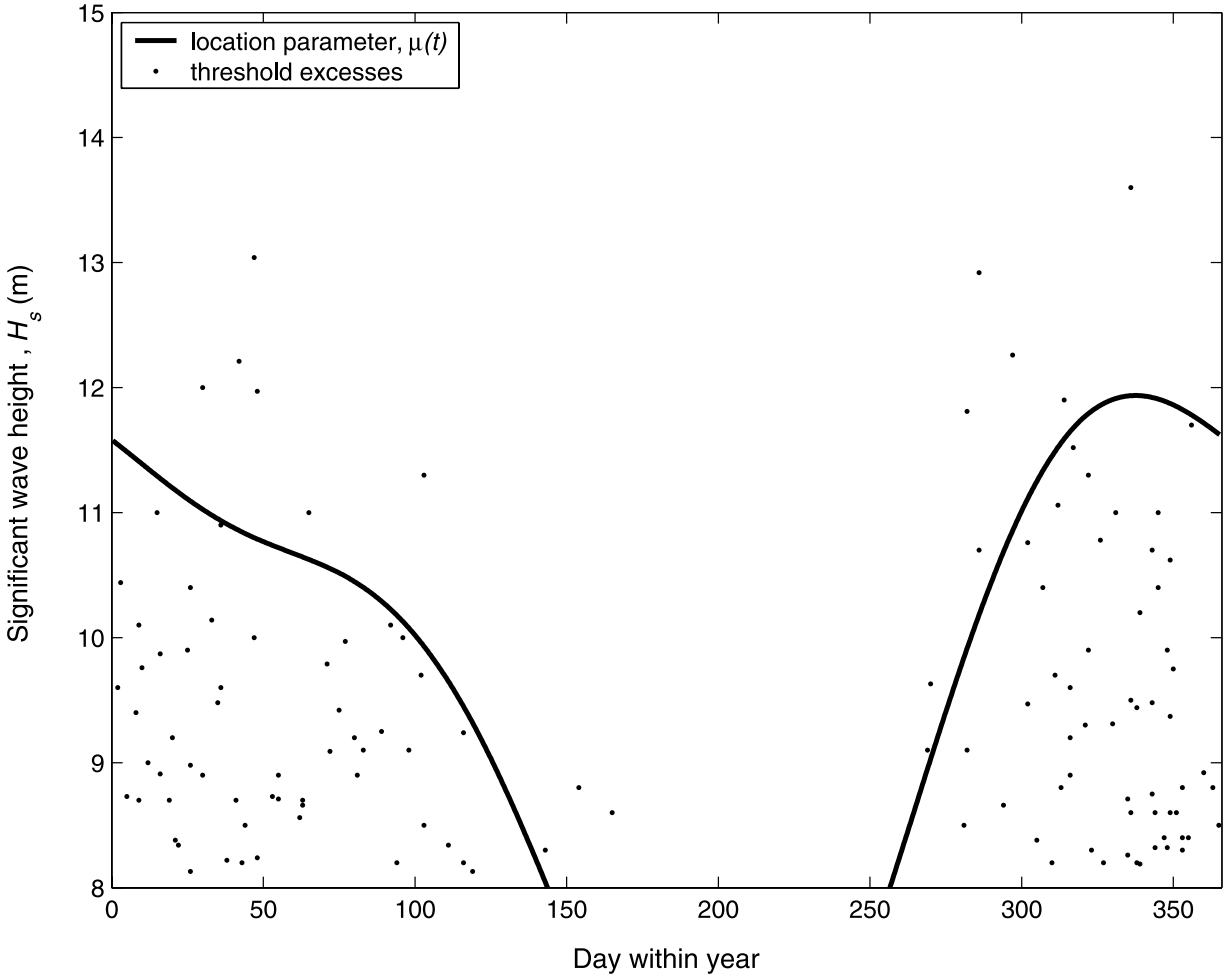

Figure 6. Estimated location parameter $\mu(t)$ for the GEV distribution of annual maxima (continuous line) and 99.5% exceedances over threshold u = 810 cm (dots) versus day within year, according to model GPD-P_4.

[43] We have also analyzed the sensitivity of the model to the selection of the threshold by selecting the 99.25 (u = 770 cm and N = 159 data) and the 99.75 (u = 880 cm and N = 76 data) percentile of the empirical H_s distribution. Compared with u = 810, the results are practically the same for u = 770 as far as β_{PNA} and β_{SOI} are concerned, whereas the long-term trend is somewhat higher ($\hat{\beta}_0\hat{\beta}_{LT}$ = 4.6 cm yr^{-1}). For u = 880, the uncertainty in the parameter estimates increases (longer confidence intervals) because of the smaller size of the sample.

5.5. Time-Dependent Parameters

[44] Figure 5 shows a comparison between the empirical event rate of exceedances (bar plot) versus the estimated event rate $\hat{\nu}(t)$ in an average year for model GPD-P_4 (continuous line) where $\hat{\nu}(t)$ is obtained from equation (4) using the ML estimates. By simple inspection, one can see that this model is able to reproduce the shape of the frequency plot very accurately.

[45] Model GPD-P_4 is also able to reproduce the seasonality of the extreme H_s amplitudes. Figure 6 shows all the threshold excesses (dots) versus the ML estimates of the time-dependent location parameter $\mu(t)$ for GPD-P_4 model in an average year (continuous line). The results show a clear seasonality in the times of high exceedances, with many fewer exceedances during the summer months. The inclusion of the seasonality improves the fit (which is statistically confirmed in Table 1).

5.6. Time-Dependent Quantiles

[46] Comparison between the different models in terms of goodness of fit and significance of the parameters involved can be demonstrated by means of quantile plots, as illustrated in Figure 7 for the time-dependent 50-year return period quantile value of the distribution of the annual maxima for the year 1992 (q = 1/50 = 0.02 in equation (12)). Solid lines represent quantile estimates, $\hat{y}_{0.02}(t)$, and dashed lines stand for the 95% confidence intervals, [$\hat{y}_{0.02}(t)$ − 1.96 *se* ($\hat{y}_{0.02}(t)$), $\hat{y}_{0.02}(t)$ + 1.96 *se* ($\hat{y}_{0.02}(t)$)]. We have added to this figure the monthly maximum values (circles) to demonstrate the seasonal behavior of the extreme values (note however that the circles and the lines are not directly comparable because the former represent monthly maxima whereas the latter correspond to annual maxima). Models GPD-P_0 and GEV_0 do not consider seasonality, but the former produces smaller confidence intervals because the

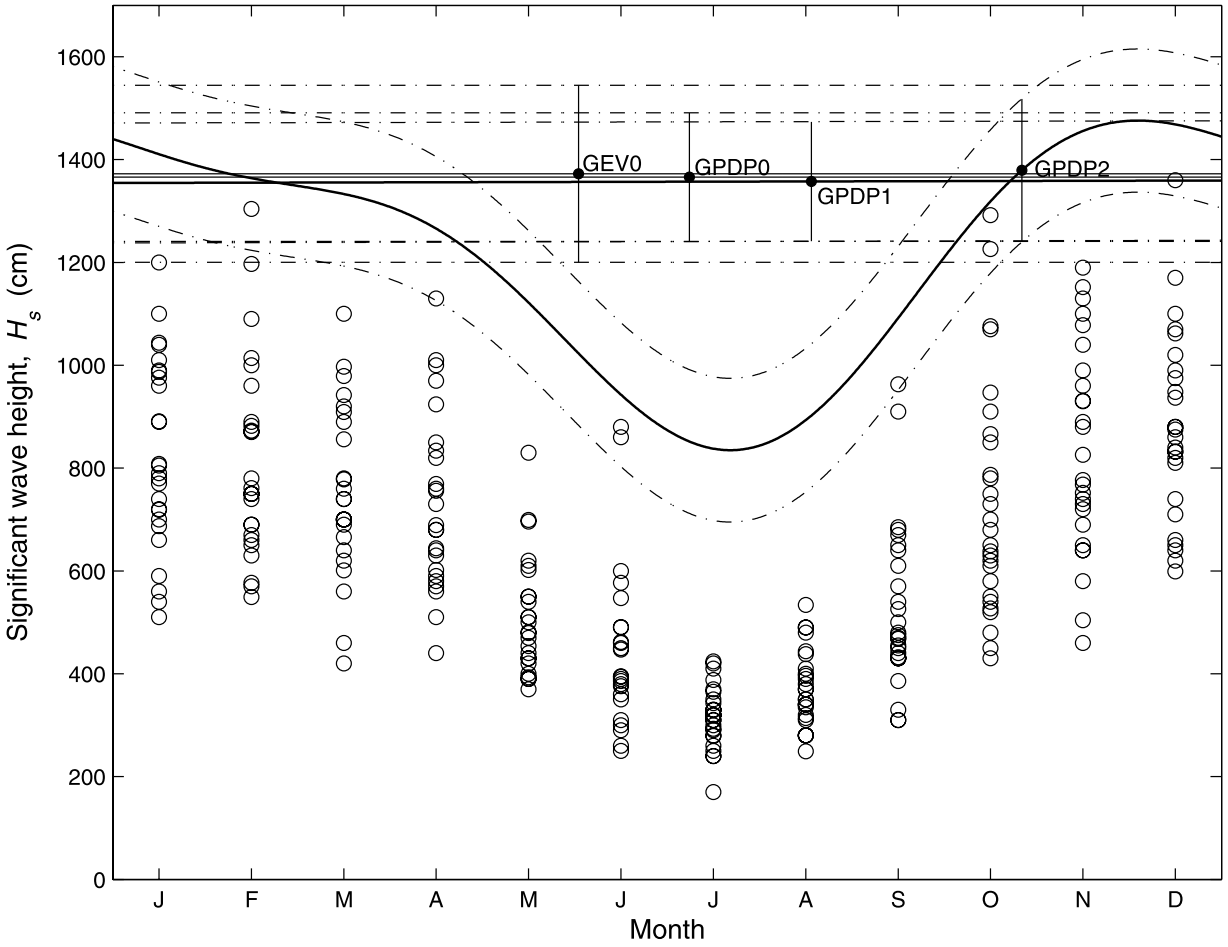

Figure 7. Comparison of estimated time-dependent 50-year return period quantiles for the GEV distribution of annual maxima evaluated at the year 1992 (continuous lines) with their confidence bands (dashed lines) for the indicated models, versus month within year. Circles represent monthly maximum values.

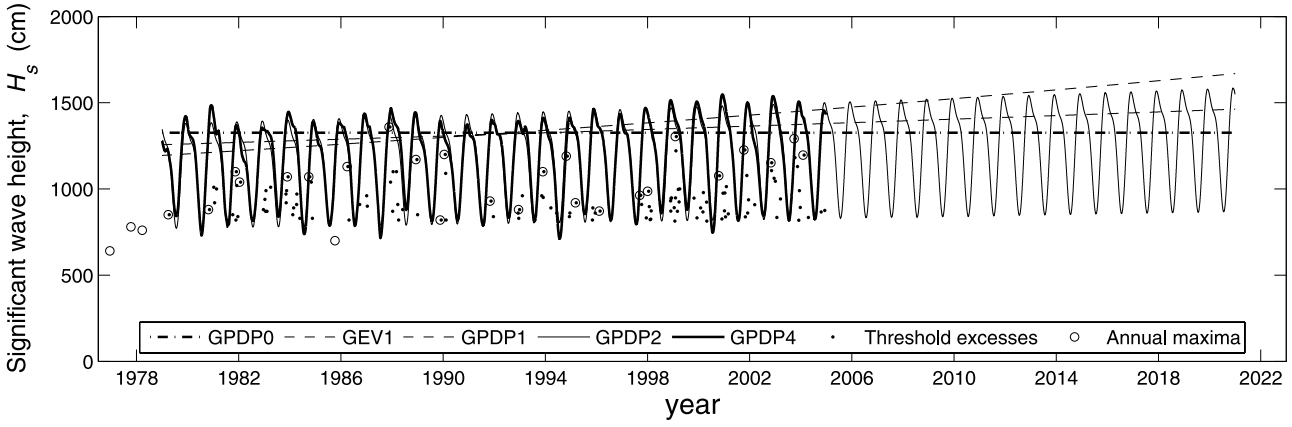

Figure 8. Comparison of 25-year quantiles time evolution and predictions from 2004 on, for the GEV distribution of annual maxima. Dots indicate exceedances over the 99.5% quantile of the empirical distribution of H_s. Annual maxima are indicated by circles.

estimates are based on 125 data rather than simply on the 23 annual maxima. The inclusion of the long-term trend in model GPD-P_1 further improves the goodness of fit, as indicated by the still smaller confidence interval. The introduction of seasonality (using model GPD-P_2) helps to reproduce the variability along the year of the monthly extreme values and produces a dramatic decrease in the point estimates and confidence intervals corresponding to the summer season which is counterbalanced by a relatively small "increase" during winter.

[47] Finally, the evolution of the 25-year return period H_s quantile is shown in Figure 8 for the different models considered. As in Figure 3, annual maxima H_s (circles) and exceedances over the 99.5% quantile of the empirical H_s distribution (dots) are shown. A horizontal dotted dashed line represents the constant quantile for GPD-P_0 model. The long-term trend estimated from model GPD-P_1 (4.4 cm yr^{-1}; dashed line) is smaller than that from GEV_1 (8.5 cm yr^{-1}; grey dashed line). Models GPD-P_2 (3.5 cm yr^{-1}; solid line) and GPD-P_4 (3.2 cm yr^{-1}; bold line) are able to reproduce not only the long-term trends, but also seasonality. Moreover, GPD-P_4 simulates the interannual climate variability, which does not affect the long-term trend estimation (see Table 1). It is important to note that the GPD-P_4 model is not extrapolated to the year 2020 since the uncertainty of the long-term prediction of the PNA and the SOI indices is very high. Moreover, the long-term trend prediction should be analyzed with caution since the Pacific decadal variability (in terms of the PDO) is not considered in the model.

6. Conclusions

[48] A statistical model to estimate long-term trends in the frequency and intensity of severe storm waves is presented in this paper. The model is based on a time-dependent version of the POT model and is applied to the Washington buoy (46005) H_s data set.

[49] The inclusion in the model of time-dependent parameters such as sine waves to represent seasonal effects, exponential functions to model the long-term trend and covariates for PNA and SOI, representing the interannual climate variability, improves the goodness of fit of the model to the data and the significance of the model parameters, especially for the long-term trend. This is because (1) the POT model uses a number of major storms considerably larger than the number of annual maxima and (2) the seasonal-to-decadal modulations included in the model explain some variability in the data and consequently reduce the uncertainty in the determination of the long-term trend.

[50] For the particular data set analyzed (H_s measured at Washington NOAA buoy, 46005), the long-term positive trend estimate tends to decrease slightly as the number of factors in the model increases. An important conclusion is that PNA and SOI covariates practically do not affect the long-term trend estimation. Whether this trend may be expected to continue in the future is an open question that should be addressed considering the changes associated with the Pacific decadal variability.

[51] Results show that the model is appropriate for a detailed analysis of long-term trends and variability of extreme waves, providing time-dependent quantiles and confidence intervals.

[52] **Acknowledgments.** The work is partially funded by the projects ENE2004-08172 and CGL2005-05365/CLI from the Spanish Ministry of Education and Science and the Project "Wave climate duration along the Spanish littoral" from the Spanish Ministry of Public Works. Fernando J. Méndez and Melisa Menéndez are indebted to the Spanish Ministry of Education and Science for the funding provided in the "Ramon y Cajal" Program and FPI Program, respectively. Alberto Luceño acknowledges the support of the Spanish Dirección General de Investigación under grant MTM2005-00287. We thank two anonymous reviewers for helpful comments that notably improved this manuscript.

References

Akaike, H. (1973), Information theory and an extension of the maximum likelihood principle, in *Proceedings of the 2nd International Symposium on Information Theory*, edited by B. N. Petrov and F. Csáki, pp. 267–281, Akad. Kiadó, Budapest.

Allan, J. C., and P. D. Komar (2000), Are ocean wave heights increasing in eastern North Pacific?, *Eos Trans. AGU*, *47*, 561–567.

Beguería, S. (2005), Uncertainties in partial duration series modelling of extremes related to the choice of the threshold value, *J. Hydrol.*, *303*, 215–230.

Bromirski, P. D., D. R. Cayan, and R. E. Flick (2005), Wave spectral energy variability in the northeast Pacific, *J. Geophys. Res.*, *110*, C03005, doi:10.1029/2004JC002398.

Carter, D. J. T., and P. G. Challenor (1981), Estimating return values of environmental variables, *Q. J. R. Meteorol. Soc.*, *107*, 259–266.

Carter, D. J. T., and L. Draper (1988), Has the northeast Atlantic become rougher?, *Nature*, *332*, 494.

Chen, T.-C., and J. Yoon (2002), Interdecadal variation of the North Pacific wintertime blocking, *Mon. Weather Rev.*, *130*, 3136–3143.

Coles, S. G. (2001), *An Introduction to Statistical Modelling of Extreme Values*, Springer, New York.

Corti, S., A. Giannini, S. Tiabldi, and F. Molteni (1997), Patterns of low-frequency variability in a three-level quasi-geostrophic model, *Clim. Dyn.*, *13*, 883–904.

Davison, A. C., and R. L. Smith (1990), Models for exceedances over high thresholds (with discussion), *J. R. Stat. Soc., Ser B*, *52*, 393–442.

Duan, Q., S. Sorooshian, and V. Gupta (1992), Effective and efficient global optimization for conceptual rainfall-runoff models, *Water Resour. Res.*, *28*, 1015–1031.

Gower, J. F. R. (2002), Temperature, wind and wave climatologies, and trends from marine meteorological buoys in the northeast Pacific, *J. Clim.*, *15*, 3709–3717.

Graham, N. E., and H. F. Diaz (2001), Evidence for intensification of North Pacific winter cyclones since 1948, *Bull. Am. Meteorol. Soc.*, *82*, 1869–1893.

Grevemeyer, I., R. Herber, and H.-H. Essen (2000), Microseismological evidence for a changing wave climate in the northeast Atlantic Ocean, *Nature*, *408*, 349–352.

Guedes Soares, C., and M. G. Scotto (2004), Application of the r largest-order statistics for long-term predictions of significant wave height, *Coastal Eng.*, *51*, 387–394.

Gulev, S. K., and V. Grigorieva (2004), Last century in ocean wind wave height from global visual wave data, *Geophys. Res. Lett.*, *1*, L24302, doi:10.1029/2004GL021040.

Hasselmann, K., D. B. Ross, P. Müller, and W. Sell (1976), A parametric prediction model, *J. Phys. Oceanogr.*, *10*, 1264–1280.

Hosking, J. R. M. (1990), L-moments: Analysis and estimation of distribution using linear combinations of order statistics, *J. R. Stat. Soc., Ser. B*, *52*, 105–124.

Hosking, J. R. M., and J. R. Wallis (1987), Parameter and quantile estimation for the Generalized Pareto distribution, *Technometrics*, *29*, 339–349.

Hurrell, J. (1995), Decadal trends in the North Atlantic Oscillation: Regional temperatures and precipitation, *Science*, *269*, 676–679.

Katz, R. W., M. B. Parlange, and P. Naveau (2002), Statistics of extremes in hydrology, *Adv. Water Resour.*, *25*, 1287–1304.

Komar, P. D., and J. C. Allan (2004), Climate controls on U.S. west coast wave heights and tide levels: Ramifications to erosion impacts, *Coastal Engineering 2004: Proceedings of the 29th International Conference*, edited by J. M. Smith. p. 223, World Sci., Hackensack, N. J.

Luceño, A., M. Menéndez, and F. J. Méndez (2006), The effect of temporal dependence on the estimation of the frequency of extreme ocean climate events, *Proc. R. Soc.*, *462*, 1683–1697.

Mantua, N. J., S. R. Hare, Y. Zhang, J. M. Wallace, and R. C. Francis (1997), A Pacific interdecadal climate oscillation with impacts on salmon production, *Bull. Am. Meteorol. Soc.*, *78*, 1069–1079.

McPhaden, M. J. (2004), Evolution of the 2002/03 El Niño, *Bull. Am. Meteorol. Soc.*, *85*, 677–695.

Morton, I. D., J. Bowers, and G. Mould (1997), Estimating return period wave heights and wind speeds using a seasonal point process model, *Coastal Eng.*, *31*, 305–326.

Pickands, J. (1975), Statistical inference using extreme order statistics, *Ann. Stat.*, *3*, 119–131.

Rice, J. (1994), *Mathematical Statistics and Data Analysis*, 2nd ed., Duxbury, Pacific Grove, Calif.

Smith, R. L. (2001), Environmental statistics, technical report, Dep. of Stat., Univ. of N. C., Chapel Hill.

Vikebo, F., T. Furevik, G. Furnes, N. Gunnar Kvamsto, and M. Reistad (2003), Wave height variations in the North Sea and on the Norwegian Continental Shelf, 1881–1992, *Cont. Shelf Res.*, *23*, 251–263.

Wallace, J. M., and D. S. Gutzler (1981), Teleconnections in the geopotential height field during the Northern Hemisphere winter, *Mon. Weather Rev.*, *109*, 784–812.

Wang, X. L., and V. R. Swail (2001), Changes of extreme wave heights in Northern Hemisphere oceans and related atmospheric circulation regimes, *J. Clim.*, *14*, 2204–2221.

I. J. Losada, F. J. Méndez, and M. Menéndez, Ocean and Coastal Research Group, Universidad de Cantabria, Avda. de los Castros s/n, E-39005 Santander, Spain. (losadai@unican.es; mendezf@unican.es; melisa.menendez@alumnos.unican.es)

A. Luceño, Department of Applied Mathematics, Universidad de Cantabria, Avda. de los Castros s/n, E-39005 Santander, Spain. (lucenoa@unican.es)